Acta Pharmaceutica Sinica B 2025;15(3):1430−1446

Chinese Pharmaceutical Association
Institute of Materia Medica, Chinese Academy of Medical Sciences

Acta Pharmaceutica Sinica B

www.elsevier.com/locate/apsb
www.sciencedirect.com

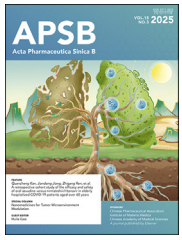

ORIGINAL ARTICLE

Parabacteroides distasonis promotes liver regeneration by increasing β-hydroxybutyric acid (BHB) production and BHB-driven STAT3 signals

Manlan Guo[a,†], Xiaowen Jiang[a,†], Hui Ouyang[a,†], Xianglong Zhang[b], Shuaishuai Zhang[a], Peng Wang[a], Guofang Bi[a], Ting Wu[a], Wenhong Zhou[a], Fengting Liang[a], Xiao Yang[a,c], Shicheng Fan[a], Jian-hong Fang[a], Peng Chen[b,*], Huichang Bi[a,c,*]

[a]*NMPA Key Laboratory for Research and Evaluation of Drug Metabolism & Guangdong Provincial Key Laboratory of New Drug Screening & Guangdong-Hongkong−Macao Joint Laboratory for New Drug Screening, School of Pharmaceutical Sciences, Southern Medical University, Guangzhou 510515, China*
[b]*Department of Pathophysiology, Guangdong Provincial Key Laboratory of Proteomics, School of Basic Medical Sciences, Southern Medical University, Guangzhou 510515, China*
[c]*The State Key Laboratory of Chemical Oncogenomics, School of Chemical Biology and Biotechnology, Shenzhen Graduate School of Peking University, Shenzhen 518055, China*

Received 1 August 2024; received in revised form 4 December 2024; accepted 20 December 2024

KEY WORDS

Liver regeneration;
Gut microbiota;
Parabacteroides distasonis;
β-hydroxybutyric acid

Abstract The liver regenerative capacity is crucial for patients with end-stage liver disease following partial hepatectomy (PHx). The specific bacteria and mechanisms regulating liver regeneration post-PHx remain unclear. This study demonstrated dynamic changes in the abundance of *Parabacteroides distasonis* (*P. distasonis*) post-PHx, correlating with hepatocyte proliferation. Treatment with live *P. distasonis* significantly promoted hepatocyte proliferation and liver regeneration after PHx. Targeted metabolomics revealed a significant positive correlation between *P. distasonis* and β-hydroxybutyric acid (BHB), as well as hyodeoxycholic acid and 3-hydroxyphenylacetic acid in the gut after PHx. Notably, treatment with BHB, but not hyodeoxycholic acid or 3-hydroxyphenylacetic acid, significantly promoted hepatocyte proliferation and liver regeneration in mice after PHx. Moreover, STAT3 inhibitor Stattic attenuated the

*Corresponding authors.
E-mail addresses: bihchang@smu.edu.cn (Huichang Bi), perchen@smu.edu.cn (Peng Chen).
[†]These authors made equal contributions to this work.
Peer review under the responsibility of Chinese Pharmaceutical Association and Institute of Materia Medica, Chinese Academy of Medical Sciences.

https://doi.org/10.1016/j.apsb.2025.01.024

promotive effects of BHB on cell proliferation and liver regeneration both *in vitro* and *in vivo*. Mechanistically, *P. distasonis* upregulated the expression of fatty acid oxidation-related proteins, and increased BHB levels in the liver, and then BHB activated the STAT3 signaling pathway to promote liver regeneration. This study, for the first time, identifies the involvement of *P. distasonis* and its associated metabolite BHB in promoting liver regeneration after PHx, providing new insights for considering *P. distasonis* and BHB as potential strategies for promoting hepatic regeneration.

1. Introduction

The liver, one of the most important organs for maintaining body homeostasis, performs multiple functions such as detoxification, metabolism, biosynthesis and glycogen storage. Meanwhile, liver disease ranks as the fifth leading cause of death worldwide. In the case of liver diseases such as liver cirrhosis and end-stage liver cancer, living-donor liver transplantation and partial hepatectomy (PHx) are the most prominent treatment strategies[1]. Notably, the liver possesses unique regenerative capability[2]. Liver regeneration is crucial for the recovery of liver function after transplantation and PHx[3]. Numerous cytokines and growth factors are required for liver regeneration, and it is imperative for the precise and orderly regulation of liver regeneration[4-6]. In the past decades, most studies on the molecular mechanisms of liver regeneration have mainly focused on the liver itself. However, growing evidence suggests that gut microbiota and its metabolites play an indispensable role in tissue repair and regeneration, and the contribution of gut microbiota through the gut−liver axis to liver regeneration has only recently been appreciated[7,8]. Therefore, it is necessary to understand the involved mechanisms that control liver regeneration, including the liver-extrinsic signals mediated by the gut microbiota.

The gut microbiota refers to the entire microbial community in the gastrointestinal tract, including bacteria, archaea, fungi, protozoa, and so on[9]. The gut microbiota, as the second genome of the human body, produces a variety of bioactive small molecules that are involved in the development and regression of liver diseases through the "gut−liver axis". Therefore, modulation of the gut microbiota, including faecal microbiota transplantation (FMT), probiotics and prebiotics, has emerged as a potential therapeutic strategy[10-12]. Moreover, evidence suggests that the gut microbiota holds promise for treating liver diseases. For instance, *Lactobacillus rhamnosus GG*, *Akkermansia muciniphila*, *Bacteroides acidifaciens* and *Parabacteroides distasonis* (*P. distasonis*) have been used to prevent and improve liver fibrosis, alcoholic and nonalcoholic liver disease[13-16]. Ongoing studies have preliminarily demonstrated the dynamic changes in gut microbiota composition during liver regeneration. Meanwhile, significant time-dependent alterations in the bacterial flora have been observed following hepatectomy[17,18]. However, the detailed contributions of gut microbiota to liver regeneration, and the specific bacteria and mechanisms involved in regulating liver regeneration post-PHx remain unclear.

Therefore, the current study aimed to identify the bacterial species participating in and regulating liver regeneration and the involved mechanisms. The results demonstrated dynamic changes in the relative abundance of *P. distasonis* post-PHx, aligning with the hepatocyte proliferation kinetics. Treatment with live *P. distasonis* significantly promoted hepatocyte proliferation and liver regeneration after PHx. Targeted metabolomics screening identified a significant positive correlation between *P. distasonis* and the associated metabolite β-hydroxybutyric acid (BHB). Moreover, BHB treatment significantly promoted hepatocyte proliferation and liver regeneration in mice after PHx. Mechanistically, *P. distasonis* upregulated the expression of fatty acid oxidation-related proteins, boosted hepatic fatty acid oxidation and increased BHB levels in the liver, and then BHB activated STAT3 signaling pathway. Taken together, this study, for the first time, identified *P. distasonis* and its associated metabolite BHB could promote liver regeneration *via* the STAT3 signaling, providing novel insights for considering *P. distasonis* or BHB as potential strategies to promote hepatic regeneration.

2. Materials and methods

2.1. Chemicals and reagents

Antibodies used in this study include anti-CCNA1 (Sangon biotech, Cat# D220507, Shanghai, China), anti-CCND1 (Sangon biotech, Cat# D220509), anti-CCNE1 (Cell Signaling Technology, Cat# 2080S, Danvers, MA, USA), anti-CDK4 (Sangon biotech, Cat# D120396), anti-PPARα (Abconal, Cat# A18252, Wuhan, China), anti-CPT1α (Proteintech, Cat# 15148-1, Wuhan, China), anti-HMGCS2 (Abconal, Cat# A23545), anti-HMGCL (Sangon biotech, Cat# D122488), anti-BDH1 (Proteintech, Cat# 67448-1), anti-JAK2 (Cell Signaling Technology, Cat# 3230T), anti-Phospho-JAK2 (Cell Signaling Technology, Cat# 3771S), anti-STAT3 (Sangon biotech, Cat# D190759), anti-Phospho-STAT3 (Tyr705) (Cell Signaling Technology, Cat# 9145), anti-acetyl-Stat3 (Lys685) (Cell Signaling Technology, Cat# 2523) and anti-c-Myc (Proteintech, Cat# 67447-1). BHB was obtained from Med Chem Express (HY-113378), Stattic was purchased from Selleck (S7024).

2.2. Animal experiments

Male C57BL/6 mice (Specific pathogen-free grade, 7−8-week old) were purchased from GermPharmatech Co., Ltd. (Foshan, China) and allowed 1−2 weeks of acclimatization. Mice had free received food and water *ad libitum* and were housed in a temperature-controlled environment (22 °C) under a standard 12 h light/dark cycle. All animal procedures were approved by the Ethics Committee on the Care and Use of Laboratory Animals in Southern Medical University (Approval number: SMUL2022162).

To screen the key bacterial species during liver regeneration after PHx, the mice were randomly divided into sham control and

PHx groups. PHx group was performed according to standard procedure as previously described[19,20]. The sham operation was performed in the same manner, except that the liver was not excised. Mice were sacrificed on Days 1, 2, 5, and 7 post-PHx. Serum, liver tissues, cecum contents, and fecal samples were collected for further experiments.

To explore the essential role of *P. distasonis* in liver regeneration after PHx, the mice were pretreated with antibiotic (ABX) cocktail (vancomycin: 100 mg/kg/day, neomycin: 200 mg/kg/day, metronidazole: 200 mg/kg/day, ampicillin: 200 mg/kg/day) once daily for 3 days to gut microbiota depletion, and then were gavaged with vehicle (PBS), live *Parabacteroides merdae* (LPM, 1×10^9 cfu/200 μL per mouse in sterilized PBS), live *P. distasonis* (LPD, 1×10^9 cfu/200 μL per mouse in sterilized PBS) or heat-killed *P. distasonis* (KPD, 1×10^9 cfu/200 μL per mouse in sterilized PBS) for 1 week. Subsequently, all mice were subjected to PHx and received PBS, LPM, LPD or KPD until the end of the study. Body weight and dietary intake were monitored during the experiments. Mice were sacrificed on Days 0, 1, 2 and 5 after PHx. Serum, liver tissues, cecum contents, and fecal samples were harvested for further experiments.

To explore the essential role of BHB, hyodeoxycholic acid (HDCA) and 3-hydroxyphenylacetic acid (3HPA) in liver regeneration after PHx, the mice were intraperitoneally injected with vehicle (PBS) or BHB (50 mg/kg/day) or HDCA (25, 50, and 100 mg/kg/day) or 3HPA (25, 50, and 100 mg/kg/day) for 3 days and then subjected to PHx[21-24]. Mice were continued to be treated with PBS or BHB or HDCA or 3HPA following PHx until the end of the study. Liver tissue, serum, cecum contents and feces samples were harvested for further experiments.

To explore the role of STAT3 signaling in BHB-promoted liver regeneration after PHx, the mice were intraperitoneally injected with vehicle (PBS) or a STAT3 inhibitor Stattic (10 mg/kg/day) or BHB (50 mg/kg/day) or Stattic + BHB for 3 days and then subjected to PHx[25]. Mice were continued to be treated with PBS or Stattic or BHB or Stattic + BHB following PHx until the end of the study.

2.3. Cell culture and treatment

HepG2 (HB-8065) cells were obtained from the American Type Culture Collection (ATCC, Manassas, VA, USA) and cultured in Dulbecco's modified Eagle's medium (DMEM, Gibco) containing 10% foetal bovine serum (FBS, Gibco) and 50 μg/mL penicillin/streptomycin at standard cell culture conditions (5% CO_2, 95% air). Cells were treated with BHB solution (1, 5 and 10 mmol/L) incubated for 3 h[26]. For the effects of STAT3 inhibitors on cells, HepG2 cells were cultured with BHB and Stattic (10 μmol/L) for 3 h[27].

2.4. Microbial strain incubation

P. distasonis and *P. merdae* were purchased from the Guangdong Microbial Culture Collection Center (GDMCC 1.1564 and GDMCC 1.3922) and cultured under anaerobic conditions at 37 °C in the brain heart infusion (BHI) broth (Solarbio, Beijing, China). The strains of *P. distasonis* and *P. merdae* were identified by comparison of the 16S rRNA sequences with the NCBI reference database (https://www.ncbi.nlm.nih.gov/), and it showed 99.8% similarity to the sequence of *P. distasonis* ATCC 8503 (NCBI Reference Sequence: NC_009615.1) and 99.9% similarity to the sequence of *P. merdae* ATCC 43184 (NCBI Reference Sequence: NZ_CP102286.1). *P. distasonis* and *P. merdae* were obtained by centrifuging at 1400×*g* for 10 min at 4 °C. The bacteria were suspended in oxygen-free sterilized PBS with a final density of 1×10^9 cfu/200 μL. To heat-kill the bacteria, *P. distasonis* was suspended in oxygen-free sterilized PBS and incubated at 95 °C for 10 min.

2.5. Histological and biochemical assessment

As previously described[28,29], liver tissues were fixed in 4% paraformaldehyde for 24 h and embedded in paraffin. Paraffin-embedded tissue slides were stained with hematoxylin and eosin (H&E) staining and Ki67 antibody (Abcam, Cat# ab16667, Cambridge, UK). Olympus microscope was used to observe and obtain the pictures of stained liver sections. For Ki67 staining, the number of $Ki67^+$ cells was counted, and the percentage of $Ki67^+$ cells in the whole section was calculated and statistically analyzed. The levels of serum aspartate transaminase (AST), alanine aminotransferase (ALT), alkaline phosphatase (ALP), total bile acid (TBA) and total bilirubin (TBIL) in the mice were measured by commercially available kits (Nanjing Jiancheng Bioengineering Institute, Nanjing, China) following the manufacturer's standard protocols.

2.6. 16S rRNA sequencing

16S rRNA sequencing was conducted as in our previous reports[30,31]. Bacterial genomic was extracted from mice feces using a DNA extraction Kit (Mabio, Guangzhou, China), according to the manufacturer's protocol. The total DNA of each sample was diluted to 5 ng/μL. PCR amplification was performed for the variable region 4 (V4) region of the bacterial 16S rRNA gene containing specific barcode tags using the forward primer (5′-GTGTGYCAGCMGCCGCGGTAA-3′) and the reverse primer (5′-CCGGACTACNVGGGTWTCTAAT-3′). PCR amplification procedure: initial denaturation at 95 °C for 2 min, followed by 30 cycles of denaturation at 95 °C for 15 s, annealing at 60 °C for 1 min. 30 cycles of PCR. At the end of the PCR reaction, the PCR products were mixed according to the ΔRn value and the quality of the amplified products was evaluated by agarose gel electrophoresis. For microbial diversity analysis, the 16S rRNA V4 region was amplified and sequenced by using the Illumina NovaSeq 6000 System (Illumina), and the raw sequences were quality-controlled using QIIME2[32]. Operational taxonomic units (OTUs) were chosen by open reference OTU picking based on 97% sequence similarity to the Greengenes 13_5 database. Principal component, alpha diversity, and beta diversity analyses were performed by using QIIME2.

2.7. Targeted metabolomic analysis

Mice feces samples on Day 2 after PHx were collected and homogenized with water. Methanol-containing internal standard was used to extract the metabolites, and the samples were centrifuged at 18,000×*g* for 20 min. Then, the supernatant was used by an ultra-performance liquid chromatography coupled to tandem mass spectrometry (UPLC−MS/MS) system (ACQUITY UPLC-Xevo TQ-S, Waters Corp., Milford, MA, USA) to quantitate microbial metabolites. ACQUITY UPLC BEH C18 1.7 μm VanGuard pre-columns (2.1 mm × 5 mm) and ACQUITY UPLC BEH C18 1.7 μm analytical columns (2.1 mm × 100 mm) were used for analysis. The column temperature was 40 °C. The flow rate was

0.4 mL/min; mobile phase A = water with 0.1% formic acid; and mobile phase B = acetonitrile/isopropyl alcohol (70:30, *v:v*). The analysis was conducted as follows: 0−1 min (5% B), 1−11 min (5%−78% B), 11−13.5 min (78%−95% B), 13.5−14 min (95%−100% B), 14−16 min (100% B), 16−16.1 min (100%−5% B), 16.1−18 min (5% B). The raw data files generated by UPLC−MS/MS were processed using the TMBQ software (v1.0, Metabo-Profile, Shanghai, China) to perform peak integration, calibration, and quantitation for each metabolite. The platform iMAP (v1.0, Metabo-Profile, Shanghai, China) was used for statistical analyses.

2.8. BHB measurements

Liver, serum and *P. distasonis* culture medium samples were collected to measure the BHB levels. Liver tissues were extracted in a homogenizer at 5000 rpm for 30 s in RIPA lysis buffer (Thermo Scientific, MA, USA). Serum and *P. distasonis* culture medium samples were obtained by centrifugation. BHB levels were detected in serum by colorimetric assay according to the manufacturer's instructions. Data were normalized to total protein content as detected by BCA assay (Thermo Scientific, MA, USA).

2.9. Proteomic LC−MS/MS analysis

Following the filter-aided sample preparation (FASP) protocol, liver tissues were digested and subjected to LC−MS/MS analysis using a Q Exactive HF-X mass spectrometer (ThermoFisher Scientific, MA, USA).

The peptide samples were separated using the NanoElute UPLC system (ThermoFisher Scientific, MA, USA). Solvent A is a solution of 0.1% formic acid and 2% acetonitrile in water, and Solvent B is a solution of 0.1% formic acid and 100% acetonitrile. The liquid phase gradient was set as follows: 0−70 min, 6%−24% B; 70−82 min, 24%−35% B; 82−86 min, 35%−80% B; 86−90 min, 80% B, with a constant flow rate of 450 nL/min. The peptides were subjected to capillary source followed by the timsTOF Pro (Bruker Daltonics) mass spectrometry. The electrospray voltage applied was 1.60 kV. Precursors and fragments were analyzed at the TOF detector, with a MS/MS scan range from 100 to 1700 *m/z*. The timsTOF Pro was operated in parallel accumulation serial fragmentation (PASEF) mode. Precursors with charge states 0 to 5 were selected for fragmentation, and 10 PASEF−MS/MS scans were acquired per cycle. The dynamic exclusion was set to 30 s.

For protein identification, the raw MS/MS data were processed using MaxQuant search engine (version 1.6.15.0). Tandem mass spectra were searched against the human SwissProt database (20422 entries) concatenated with the reverse decoy database. Trypsin/P was specified as cleavage enzyme allowing up to 2 missing cleavages. The mass tolerance for precursor ions was set as 20 ppm in the first search and 5 ppm in the main search, and the mass tolerance for fragment ions was set as 0.02 Da. Carbamidomethyl on Cys was specified as a fixed modification, and acetylation on protein N-terminal and oxidation on Met were specified as variable modifications. The false discovery rate (FDR) was adjusted to $< 1\%$. The proteins with fold change (FC) > 1.2 and P value < 0.05 were considered as differentially expressed proteins (DEPs).

2.10. qRT-PCR analysis

Total RNA was isolated and cDNA was synthesized as described in our previous report[33]. Total RNA was extracted using TRIzol reagent (AG, Shanghai, China) and reverse transcribed into cDNA using Hifair one-step RT-gDNA digestion SuperMix Kit (Yeasen, Shanghai, China). Then qRT-PCR was performed on an Applied Biosystem 7500 using Hieff qPCR SYBR Green Master Mix kit (Yeasen, Shanghai, China) following the instructions from the manufacturer. The fold changes of mRNA levels were calculated by the ΔΔCt method. All primer sequences used for qRT-PCR are listed in Supporting Information Table S1.

2.11. Western blotting

Western blot analysis was conducted according to our previous report[19]. For total protein extraction, liver tissues were homogenized with RIPA lysis buffer containing 1 mmol/L PMSF and phosphatase inhibitors. BCA Protein Assay Kit (Thermo Scientific, Rockford, IL, USA) was used to quantify protein concentration. Protein samples were separated by SDS-PAGE gel and transferred onto polyvinylidene difluoride membranes (Millipore). The membranes were blocked in 5% milk for 1 h at room temperature. Then the membranes were incubated with different antibodies 4 °C for overnight. After incubation with a secondary antibody, the immunoblotting was evaluated using enhanced chemiluminescence (ECL) kit (Millipore, Darmstadt, Germany) and a Bio-Rad systems. The immunoblot intensity was quantified using Image J software.

2.12. ELISA assays

The protein levels of hepatic IL-6 were measured by commercial ELISA kits obtained from Neobioscience (EMC004.96, Shenzhen, China).

2.13. Statistical analysis

All statistical analyses in this study were performed using GraphPad Prism 8.4.0 software (GraphPad Software, San Diego, USA). All data are expressed as the mean ± standard deviation (SD). Unpaired *t* tests or one-way ANOVA was used to assess the differences between groups using SPSS 23.0 software (IBM Analytics). Taxonomic comparisons from 16S rRNA sequencing analysis were analyzed by Kruskal−Wallis test with Bonferroni *post hoc* test. Correlations between cecal metabolites and *P. distasonis* abundance were evaluated using Spearman's rank correlation analysis. Differences with P values < 0.05 were considered significant.

2.14. Data availability statement

The 16S data have been deposited in the Genome Sequence Archive (GSA): CRA013483. The metabolome and mass spectrometry proteomics data have been deposited in the OMIX (Open Archive for Miscellaneous Data): OMIX005186 and OMIX005187.

3. Results

3.1. Liver regeneration after PHx in mice

After PHx, the liver/body weight ratio was almost restored to its original size on Day 7 (Supporting Information Fig. S1A−S1C), consistent with our previously reported findings[19]. H&E staining showed no apparent liver injury during liver regeneration post-

PHx. Ki67 immunostaining of liver sections revealed that hepatocyte proliferation was started on Day 1 post-PHx, peaked on Day 2, and significantly decreased on Day 7 (Fig. S1D and S1E). The serum levels of AST, ALT, ALP, TBIL, and TBA were also strongly elevated on Day 1 post-PHx and returned to their normal levels on Day 7 (Fig. S1F).

3.2. *Alteration in gut microbiota during liver regeneration*

To reveal the alteration in gut microbiota during liver regeneration and identify the bacterial species associated with liver regeneration, 16S rRNA sequencing was performed using mice feces. The results showed that operational taxonomic unit (OTU) diversities were not significantly altered during liver regeneration post-PHx (Supporting Information Fig. S2A); however, there was a distinct change in gut microbiota composition (Fig. 1A). Moreover, there was a shift in the composition of gut microbiota at the phylum level during the process of liver regeneration (Fig. 1B and Fig. S2B). At the genus level, compared to the sham group, the relative abundance of *Parabacteroides* was significantly increased on Day 1, and gradually decreased but remained significantly enriched on Days 2 and 5, and returned to normal levels on Day 7 post-PHx (Fig. 1C). Meanwhile, the relative abundance of *Bacteroides* significantly increased on Day 1, reaching the peak, and then returned to normal levels on Days 5−7 post-PHx. In contrast, the relative abundance of *Lactobacillus* significantly decreased at all time points after PHx (Fig. 1C). MaAsLin2 analysis identified 15 gut microbiota genera significantly associated with liver regeneration. *Bacteroides* showed a significant positive correlation with liver regeneration on Days 1 and 2. *Parabacteroides* exhibited a significant positive correlation with liver regeneration on Days 1 and 2, and a significant negative correlation on Day 5, which was consistent with the relative abundance of *Parabacteroides* during liver regeneration post-PHx. Furthermore, *Akkermansia* and *Turicibacter* showed significant negative correlations with liver regeneration (Fig. S2C, Supporting Information Table S2).

We further analyzed the distribution characteristics of these enriched genera at the species level using qPCR. The relative abundance of *P. merdae* was significantly increased at all time points after PHx, with the most significant increase observed on Day 5. There were no significant differences in the relative abundance of *Parabacteroides goldsteinii*, *Bacteroides vulgatus*, and *Bacteroides dorei* at all time points after PHx. However, compared to the sham group, the relative abundance of *P. distasonis* in mice feces was significantly increased on Day 1, reaching a peak, decreased on Day 2 but remained significantly higher than the sham group, and returned to normal levels on Day 7 post-PHx, which was aligned with the hepatocyte proliferation kinetics after PHx (Fig. 1D, Fig. S1D and S1E). These data suggest that the relative abundance of *P. distasonis* is positively correlated with hepatocyte proliferation during the regeneration process, indicating that *P. distasonis* may play an important role as a specific bacterium during liver regeneration after PHx.

3.3. *Treatment with live P. distasonis promotes liver regeneration after PHx*

To further clarify the role of specific key bacteria in liver regeneration, C57BL/6 mice were subjected to PHx and were orally administered the vehicle (PBS), live *P. distasonis* (LPD) or heat-killed *P. distasonis* (KPD). Firstly, the relative abundance of *P. distasonis* in the intestines was examined following oral gavage LPD or KPD. The results showed a significant enrichment of *P. distasonis* in the cecum contents and feces of mice gavaged with LPD for 7 days, while the relative abundance of the KPD-treated group remained unchanged, indicating that live *P. distasonis* can colonize and survive in the mouse intestines (Supporting Information Fig. S3A). Furthermore, we found that LPD treatment significantly increased liver size and liver/body weight ratio on Days 2 and 5 post-PHx (Fig. 2A−C). H&E staining and serum AST, ALT, ALP, TBIL and TBA measurement showed no apparent liver injury after LPD or KPD treatment (Fig. 2D and Fig. S3B). The number of $Ki67^{+}$ hepatocytes was substantially increased after LPD treatment (Fig. 2E and F). In addition, LPD treatment significantly upregulated levels of the proliferation-related proteins, including CCNA1, CCND1 and CDK4 post-PHx (Fig. 2G and Supporting Information Fig. S4). Meanwhile, since the relative abundance of *P. merdae* was significantly increased at all time points after PHx, we further investigated whether live *P. merdae* (LPM) could induce liver regeneration (Supporting Information Fig. S5A). The results show a significant enrichment of *P. merdae* in the cecum contents and feces of mice gavaged with live *P. merdae* for 7 days, indicating a successful colonization of *P. merdae* in the intestine (Fig. S5B). However, *P. merdae* treatment did not increase liver size or the liver/body weight ratio after PHx (Fig. S5C and S5D). Moreover, H&E staining and measurement of serum AST, ALT, ALP, TBIL and TBA showed no apparent liver injury after treatment with live *P. merdae* (Fig. S5E and S5F).

In conclusion, these findings collectively suggested that the administration of live *P. distasonis* accelerated liver regeneration after PHx by promoting hepatocyte proliferation, but treatment with live *P. merdae* could not promote liver regeneration after PHx.

3.4. *P. distasonis increases BHB production in cecum contents and liver after PHx*

To reveal the potential involvement of the associated metabolites during the alterations of gut microbiota composition, targeted metabolomics quantified more than 300 metabolites to identify metabolites significantly associated with *P. distasonis*. The analysis revealed prominently different metabolites in the cecum contents between the vehicle-treated and the LPD-treated groups. As shown in Fig. 3A, principal component analysis (PCA) demonstrated a notable shift in the metabolic profiles of gut microbiota in *P. distasonis*-treated mice, compared with the vehicle group. We found that 34 metabolites were significantly changed in the cecum contents of *P. distasonis*-treated mice, including hyodeoxycholic acid (HDCA), 3-hydroxyphenylacetic acid (3HPA), BHB, imidazolepropionic acid and others (Fig. 3B and C, Supporting Informaiton Table S3). Among these metabolites, BHB concentration was positively correlated with *P. distasonis* relative abundance in cecum contents. Moreover, BHB was also enriched in both liver tissue and peripheral blood serum in *P. distasonis*-treated mice after PHx (Fig. 3D and E). However, the concentration of BHB in the *P. distasonis* culture medium showed no significant difference compared to the control medium *in vitro* (Fig. 3F). These results showed that *P. distasonis* treatment significantly increased the content of BHB in cecum contents, liver and peripheral blood serum, suggesting that BHB may be involved in *P. distasonis*-induced promotion in liver regeneration after PHx.

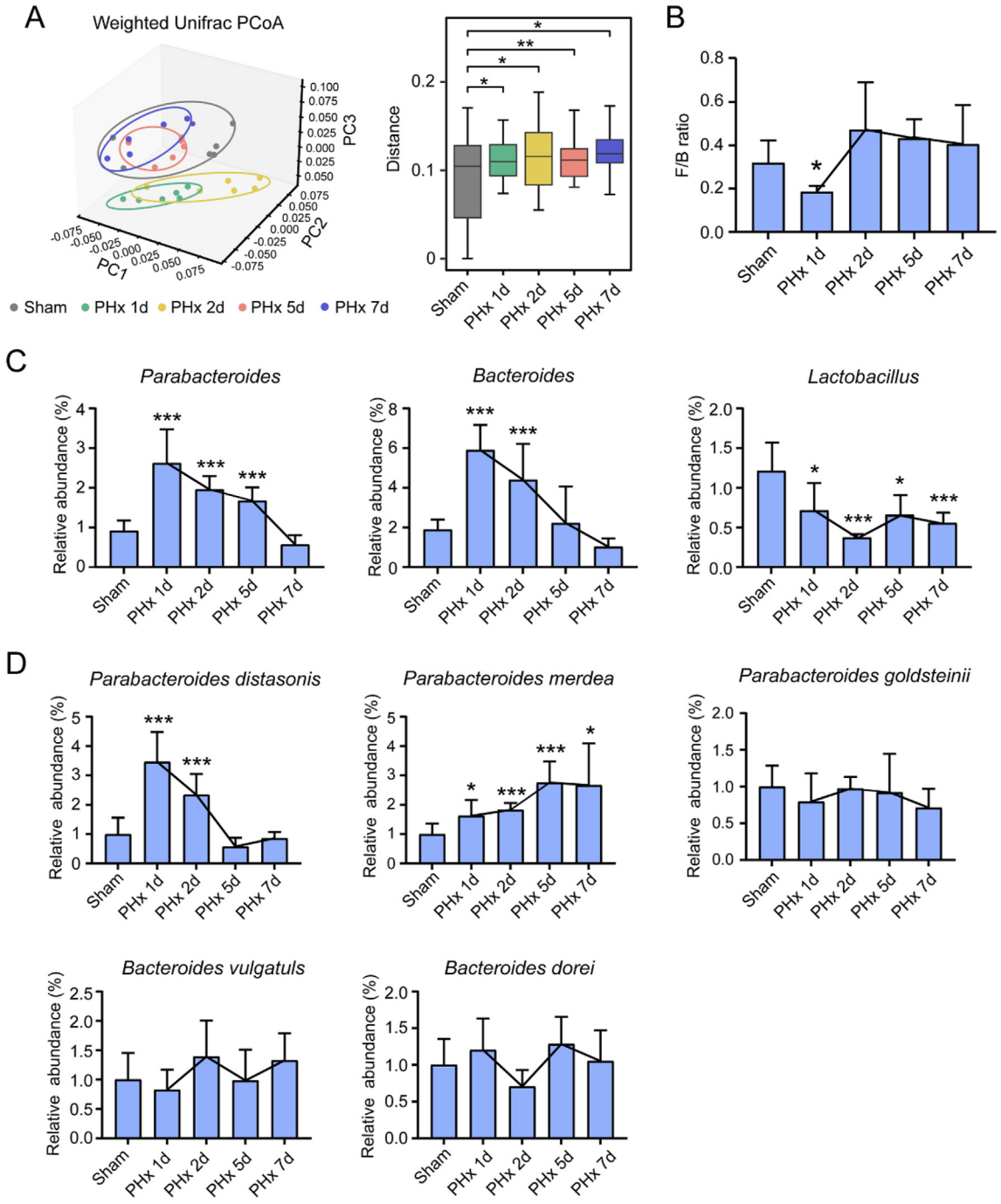

Figure 1 Gut microbiota composition is dynamically changed during liver regeneration. (A) Principal Coordinates Analysis (PCoA) plot using weighted unifrac distance. (B) *Firmicutes*/*Bacteroidetes* (F/B) ratios. (C) Relative abundance of the genera *Parabacteroides*, *Bacteroides* and *Lactobacillus* during liver regeneration. For (A–C), 16S rRNA sequencing analysis in fecal bacterial DNA was performed during the course of liver regeneration. (D) qPCR analysis shows relative abundances of *P. distasonis*, *P. merdea*, *P. goldsteinii*, *B. vulgatuls* and *B. dorei* during regeneration. Data are presented as mean ± SD, $n = 6$; $^{*}P < 0.05$, $^{***}P < 0.001$ compared to the sham group.

3.5. *BHB promotes liver regeneration after PHx*

To confirm the contribution of BHB in the vital role of *P. distasonis* in liver regeneration, C57BL/6 mice were subjected to PHx and treated with either vehicle (PBS) or BHB (Fig. 4A). The result showed that BHB treatment significantly increased the liver/body weight ratio on Days 2 and 5 post-PHx (Fig. 4B and C). No significant differences in serum levels of AST, TBIL and TBA were observed between the vehicle-treated and BHB-treated groups. However, BHB treatment significantly reduced serum ALT level on Day 2 and ALP level on Day 1 (Supporting Information Fig. S6). H&E staining revealed no apparent liver injury after BHB treatment (Fig. 4D). Immunohistochemical staining showed that BHB treatment significantly increased the

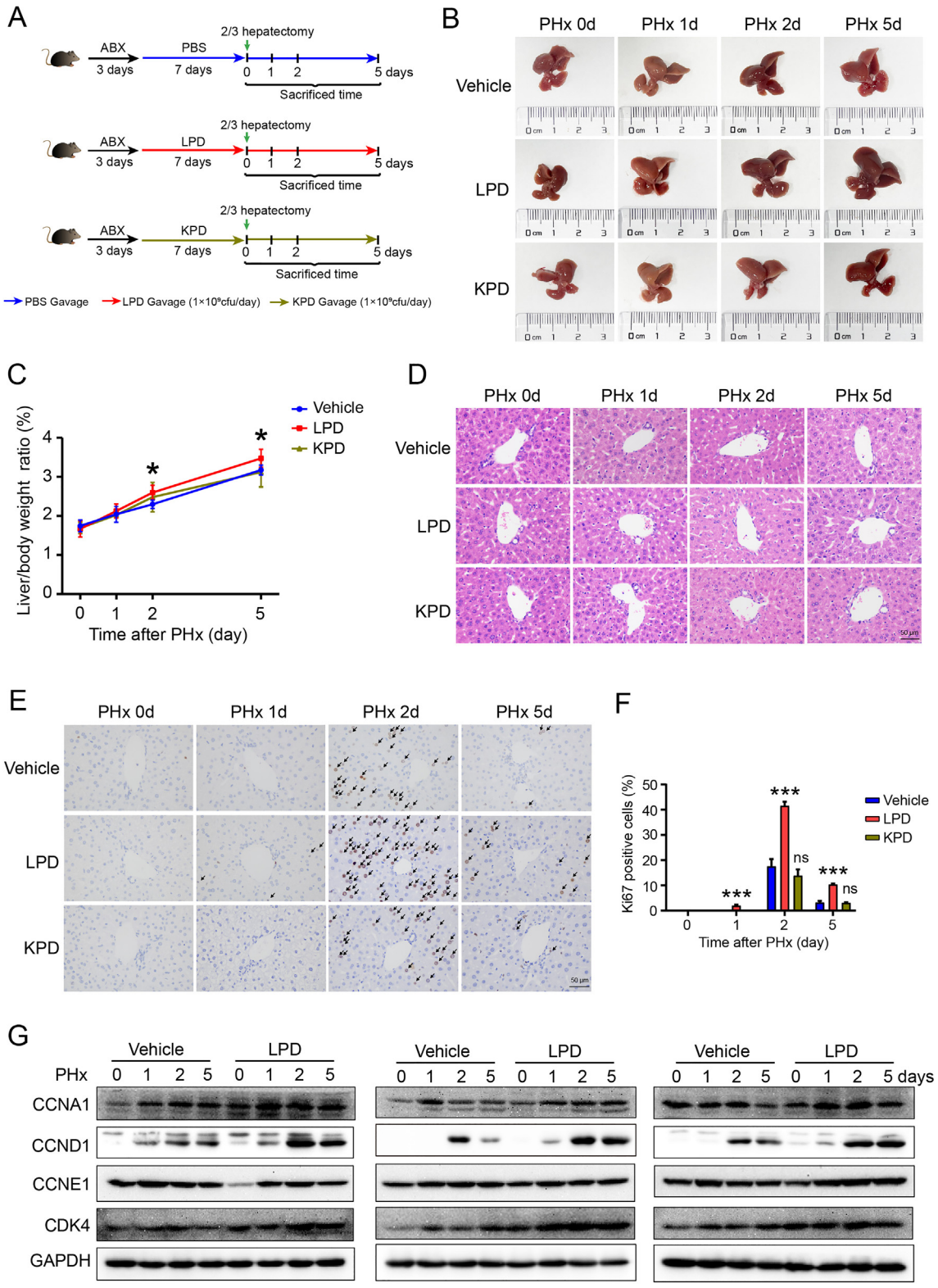

Figure 2 *P. distasonis* promotes liver regeneration post-PHx in mice. (A) Experimental scheme: mice were treated with antibiotics (vancomycin, neomycin, metronidazole and ampicillin) for 3 days. After antibiotics treatment, 1×10^9 cfu live *P. distasonis* (LPD) or heat-killed *P. distasonis* (KPD) were given by oral transplantation once a day for 1 week. Subsequently, all mice were subjected to PHx and followed by receiving 1×10^9 cfu LPD or KPD until the end of the study. (B) Representative liver images from PHx mice after vehicle, LPD or KPD treatment. (C) Liver/body weight ratios ($n = 6$). (D) H&E and (E) Ki67 staining liver tissues from PHx mice ($n = 3$). (F) Quantification of the number of Ki67$^+$ cells ($n = 3$). (G) Western blotting analysis of the proliferation-related proteins CCNA1, CCND1, CCNE1 and CDK4 in PHx mice after the vehicle or LPD administration ($n = 6$). Data are presented as mean ± SD; ns, no significant difference; $^*P < 0.05$, $^{***}P < 0.001$ compared to the vehicle group. Scale bar = 50 μm.

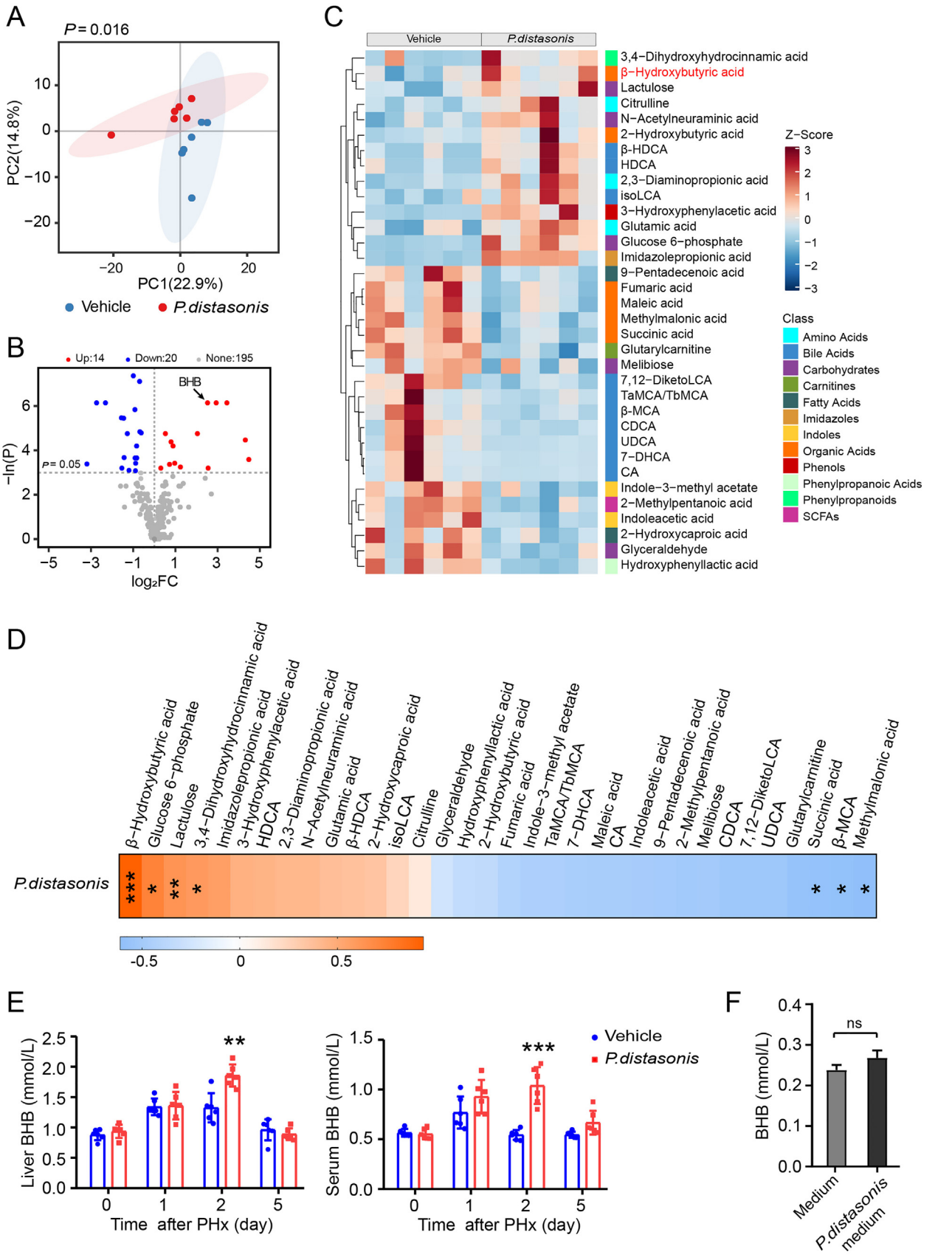

Figure 3 *P. distasonis* increases BHB production in cecum contents and liver after PHx. (A) Scatter plots of principal component analysis (PCA) for the cecal microbiota metabolomics in PHx mice on Day 2 after vehicle or LPD treatment. (B) Volcano plot of the metabolomic analysis. (C) The heatmap of intestinal microbial differential metabolites in PHx mice on Day 2 after vehicle or LPD treatment. Red represents high relative

number of Ki67-positive hepatocytes in the mouse liver tissue (Fig. 4E and F). Moreover, BHB administration upregulated the proliferation-related proteins, including CCNA1, CCND1 CCNE1 and CDK4 (Fig. 4G and Supporting Information Fig. S7) after PHx. These data indicated that BHB treatment promoted hepatocyte proliferation after PHx, thereby facilitating liver regeneration.

On the other hand, since the levels of HDCA and 3HPA were also significantly elevated in the intestinal contents of *P. distasonis*-treated mice after PHx, we further investigated whether HDCA and 3HPA could induce liver regeneration. The results showed that HDCA and 3HPA treatment did not increase the liver size and liver/body weight ratio on Day 2 post-PHx (Supporting Information Fig. S8A and S8B), suggesting that HDCA and 3HPA could not promote liver regeneration after PHx.

3.6. *P. distasonis promotes hepatic fatty acid oxidation post-PHx in mice*

To further illustrate the mechanism underlying *P. distasonis*-induced BHB production, we conducted proteomic analysis on liver tissue collected on Day 2 after PHx, comparing samples treated with or without *P. distasonis*. As shown in Supporting Information Table S4, 59 significantly differentially expressed proteins (DEPs) were identified, with 41 proteins upregulated and 18 proteins downregulated in the *P. distasonis* group. Notably, we identified significant enrichment of proliferation- and lipid metabolism-related signaling pathways through the biological process and KEGG pathway analysis of these DEPs between the *P. distasonis*-treated and vehicle-treated group (Fig. 5A and B). Moreover, our analysis of DEPs suggests potential alterations in fatty acid metabolism-associated pathways in the *P. distasonis*-treated mice post-PHx.

To further investigate whether *P. distasonis* regulates fatty acid metabolism during liver regeneration after PHx, qPCR was used to measure the mRNA levels of genes associated with fatty acid uptake, synthesis, oxidation and BHB production in liver tissue. The results showed no significant differences in the mRNA levels of genes related to fatty acid uptake, including long-chain fatty acid transport protein 1 (*Fatp*), long-chain fatty acid CoA ligase (*Acsl*), and fatty acid translocase (*Cd36*), indicating that *P. distasonis* treatment did not affect fatty acid uptake in the liver after PHx (Fig. 5C). Furthermore, there was no difference in fatty acid synthase (*Fasn*) mRNA level, while stearoyl-CoA desaturation 1 (*Scd1*) and perilipin 2 (*Plin2*) were significantly downregulated in the *P. distasonis*-treated mice on Day 2 post-PHx (Fig. 5D). Interestingly, the mRNA level of carnitine palmitoyl transferase 1α (*Cpt1a*), a gene associated with fatty acid oxidation, was significantly upregulated on Day 1 post-PHx. Proliferators-activated receptors α (*Ppara*) and long-chain specific acyl-CoA dehydrogenase (*Lcad*) mRNA levels were slightly increased on Day 1 post-PHx (Fig. 5E). Moreover, those genes related to BHB production, including hydroxymethylglutaryl-CoA synthase 2 (*Hmgcs2*), hydroxymethylglutaryl CoA lyase (*Hmgcl*) and β-hydroxybutyrate dehydrogenase 1 (*Bdh1*) were significantly upregulated in the *P. distasonis*-treated mice on Day 1 post-PHx (Fig. 5F). Consistently, we found a significant increase in protein levels of nuclear PPARα, total PPARα, CPT1A, HMGCS2, HMGCL and BDH1 in the *P. distasonis*-treated mice post-PHx (Fig. 6A and B). Taken together, these data suggested that *P. distasonis* upregulated the levels of mRNAs and proteins associated with hepatic fatty acid oxidation, contributing to BHB production and providing energy for liver regeneration after PHx.

3.7. *BHB promotes liver regeneration by activating the STAT3 signaling pathway in vitro*

BHB is not only a key energy metabolite, but also acts as an epigenetic regulator. It can elevate acetylation levels in both histone and non-histone proteins[34]. The transcription activator factor 3 (STAT3) has been implicated in liver regeneration and its transcriptional of cell growth-related genes can be modulated by acetylation modification[35,36]. Therefore, to investigate whether BHB promotes liver regeneration *via* activating the STAT3 pathway, a Western blot was performed to measure the protein expression of STAT3 in liver samples from PHx mice. The results showed that BHB treatment significantly increased the levels of phosphorylated (p-) JAK2, phosphorylated (p-) STAT3, and the STAT3 downstream target c-Myc. Additionally, BHB treatment significantly upregulated protein levels of acetylated H3 (ac-H3) and acetylated STAT3 (ac-STAT3) in the PHx mice liver (Fig. 7A, Supporting Information Fig. S9A). Furthermore, we treated HepG2 cells with BHB at different time points and found that p-STAT3 levels were most significantly elevated at 3 h post-treatment (Fig. S9B). We further treated the cells with BHB at different concentrations for 3 h. As shown, BHB treatment significantly increased the expression levels of ac-STAT3, ac-H3, p-JAK2, p-STAT3, c-Myc and CCND1 in a dose-dependent manner, consistent with *in vivo* findings (Fig. 7B and C, Fig. S9C and S9D). Notably, Stattic, a STAT3 phosphorylation inhibitor, significantly reduced the BHB-induced increases in p-JAK2, p-STAT3, c-Myc, and CCND1 levels *in vitro* (Fig. 7D, Fig. S9E). Moreover, BHB treatment upregulated IL-6 mRNA and protein levels (Supporting Information Fig. S10), a pro-inflammatory cytokine that activates the STAT3 signal. Taken together, these results suggested that BHB promoted liver regeneration by activating the STAT3 signaling pathway.

3.8. *BHB promotes liver regeneration by activating the STAT3 signaling pathway in vivo*

We further investigated whether BHB promotes liver regeneration by the STAT3 signaling pathway *in vivo*. Mice were treated with the STAT3 inhibitor Stattic to confirm the role of STAT3 signaling in BHB-induced liver regeneration (Fig. 8A). The results showed that BHB treatment significantly increased the liver/body weight ratio of mice on Days 2 and 5 post-PHx, while those of BHB + Stattic treated mice remained unchanged (Fig. 8B and C). H&E staining and AST, ALT, ALP, TBIL and TBA levels revealed no obvious liver injury after BHB and BHB + Stattic treatment (Fig. 8D, Supporting Information Fig. S11A). The number of Ki67$^+$ hepatocytes in the BHB+Stattic-treated mice was lower than that in the BHB-treated mice on Day 2 post-PHx (Fig. 8E and

abundance, while blue represents low relative abundance. (D) Heatmap of Spearman correlation coefficients between the relative LPD abundance and the differential metabolites on Day 2 post-PHx. (E) Levels of BHB in liver, serum and (F) medium samples after LPD treatment during liver regeneration. Data are presented as mean ± SD, $n = 6$; ns, no significant difference; $^{**}P < 0.01$, $^{***}P < 0.001$ compared to the vehicle group at the same time point.

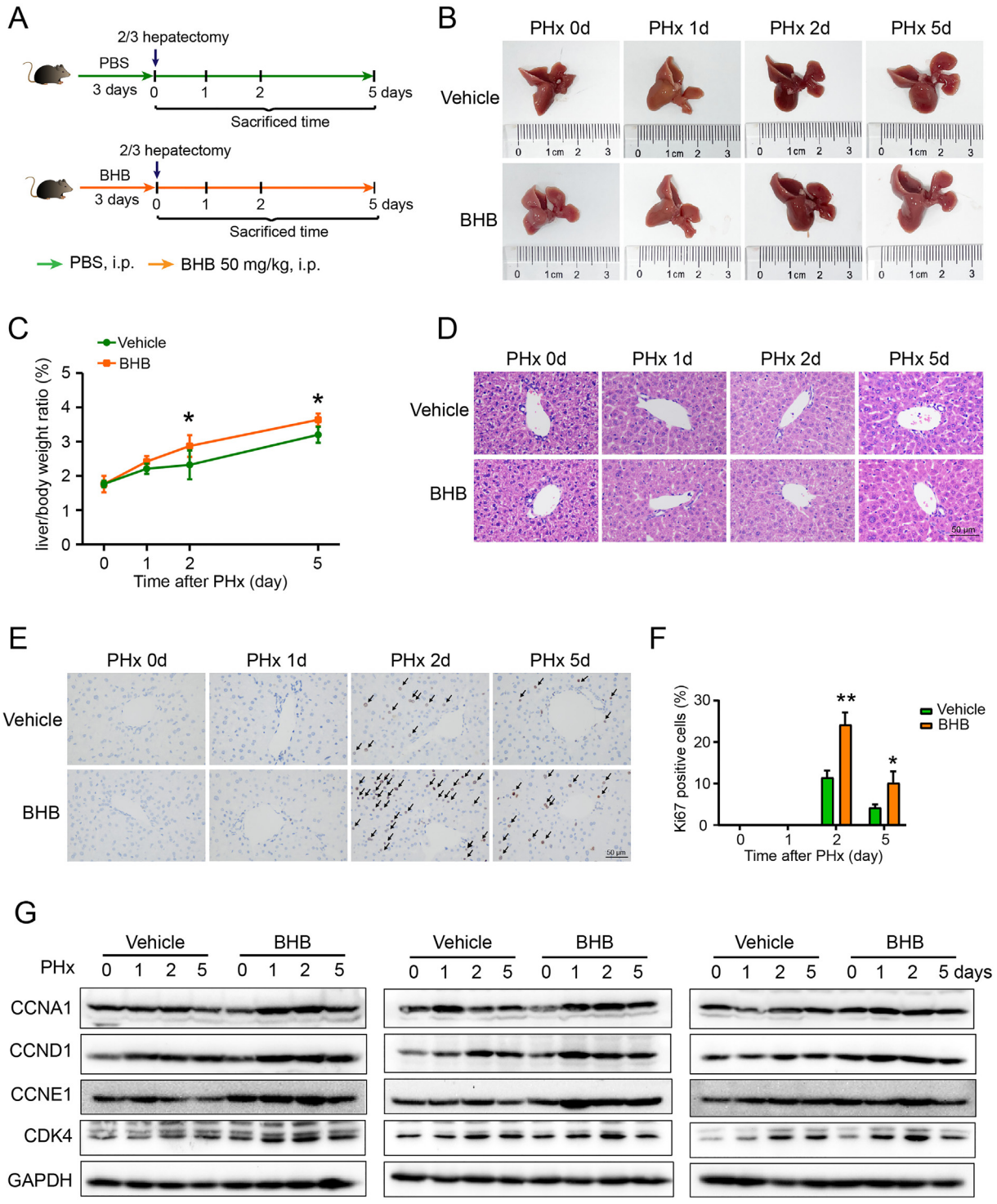

Figure 4 BHB promotes liver regeneration post-PHx in mice. (A) Experimental scheme: the mice were intraperitoneally injected with vehicle (PBS) or 50 mg/kg/day BHB for 3 days and then subjected to PHx. Mice continued to be treated with PBS or 50 mg/kg/day BHB following PHx until the end of the study. (B) Representative liver images from PHx mice after vehicle or BHB administration. (C) Liver/body weight ratios ($n = 6$), (D) H&E and (E) Ki67 staining liver tissues from PHx mice ($n = 3$). (F) Quantification of the number of $Ki67^{+}$ cells ($n = 6$). (G) Western blotting analysis of the proliferation-related proteins CCNA1, CCND1, CCNE1 and CDK4 in PHx mice after the vehicle or BHB administration ($n = 6$). Data are presented as mean ± SD;$^{*}P < 0.05$, $^{**}P < 0.01$ compared to the vehicle group at the same time point. Scale bar = 50 μm.

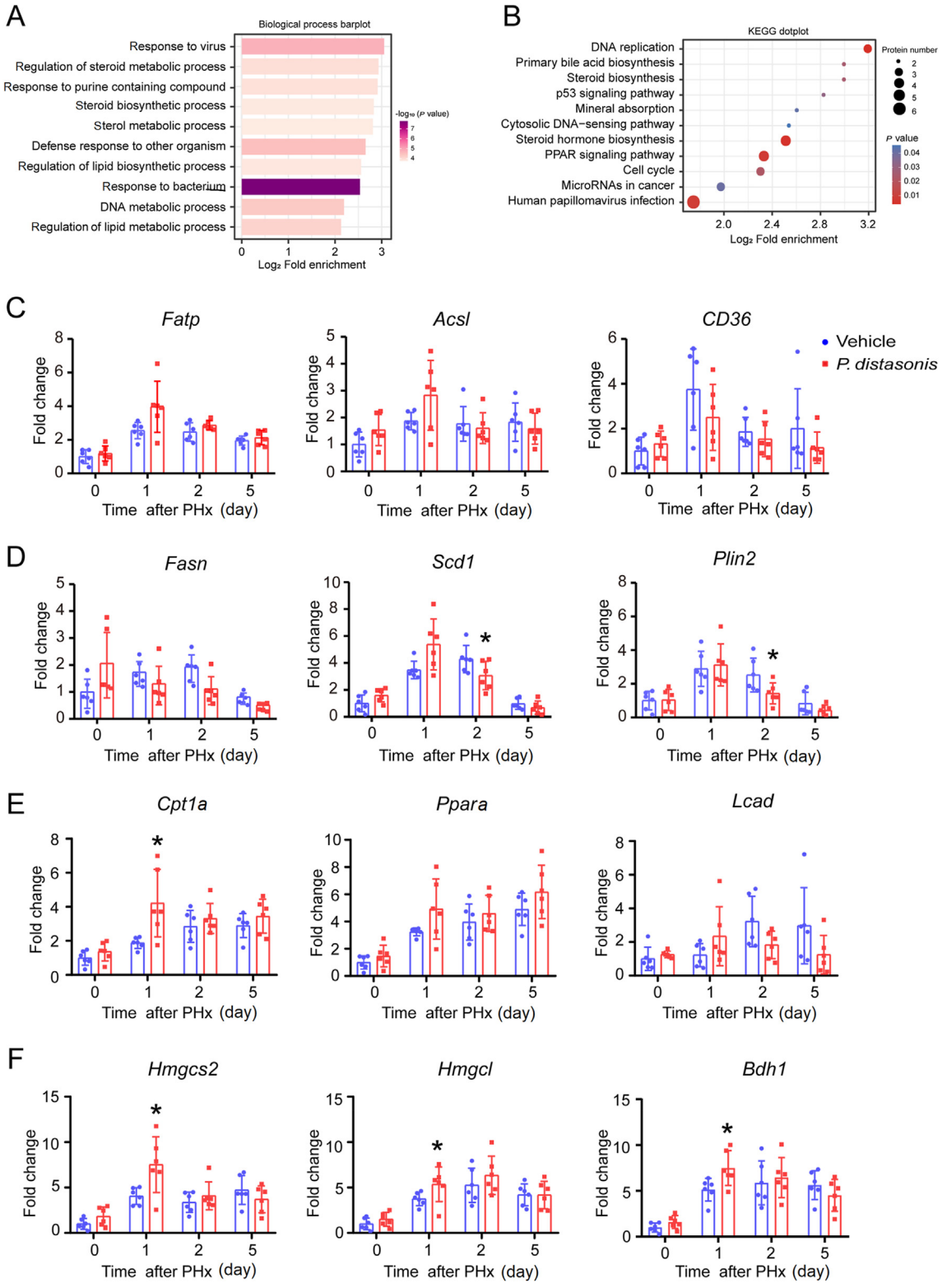

Figure 5 *P. distasonis* up-regulates mRNA levels of hepatic fatty acid oxidation related genes in livers post-PHx. (A) Biological process and (B) KEGG signaling pathway enrichment analysis reveal lipid metabolism related functional terms enriched in PHx mice on Day 2 after vehicle or LPD treatment. (C−F) qPCR analysis shows the mRNA levels of hepatic fatty acid metabolism related genes in PHx mice after vehicle or LPD treatment ($n = 6$). (C) The mRNA levels of hepatic fatty acid uptake related genes *Fatp*, *Acsl* and *Cd36*. (D) The mRNA levels of hepatic fatty acid synthesis related genes *Fasn*, *Scd1* and *Plin2*. (E) The mRNA levels of hepatic fatty acid oxidation associated genes *Cpt1a*, *Ppara* and *Lcad*. (F) The mRNA levels of BHB production associated genes *Hmgcs2*, *Hmgcl* and *Bdh1*. Data are presented as mean ± SD; $^*P < 0.05$ compared to the vehicle group at the same time point.

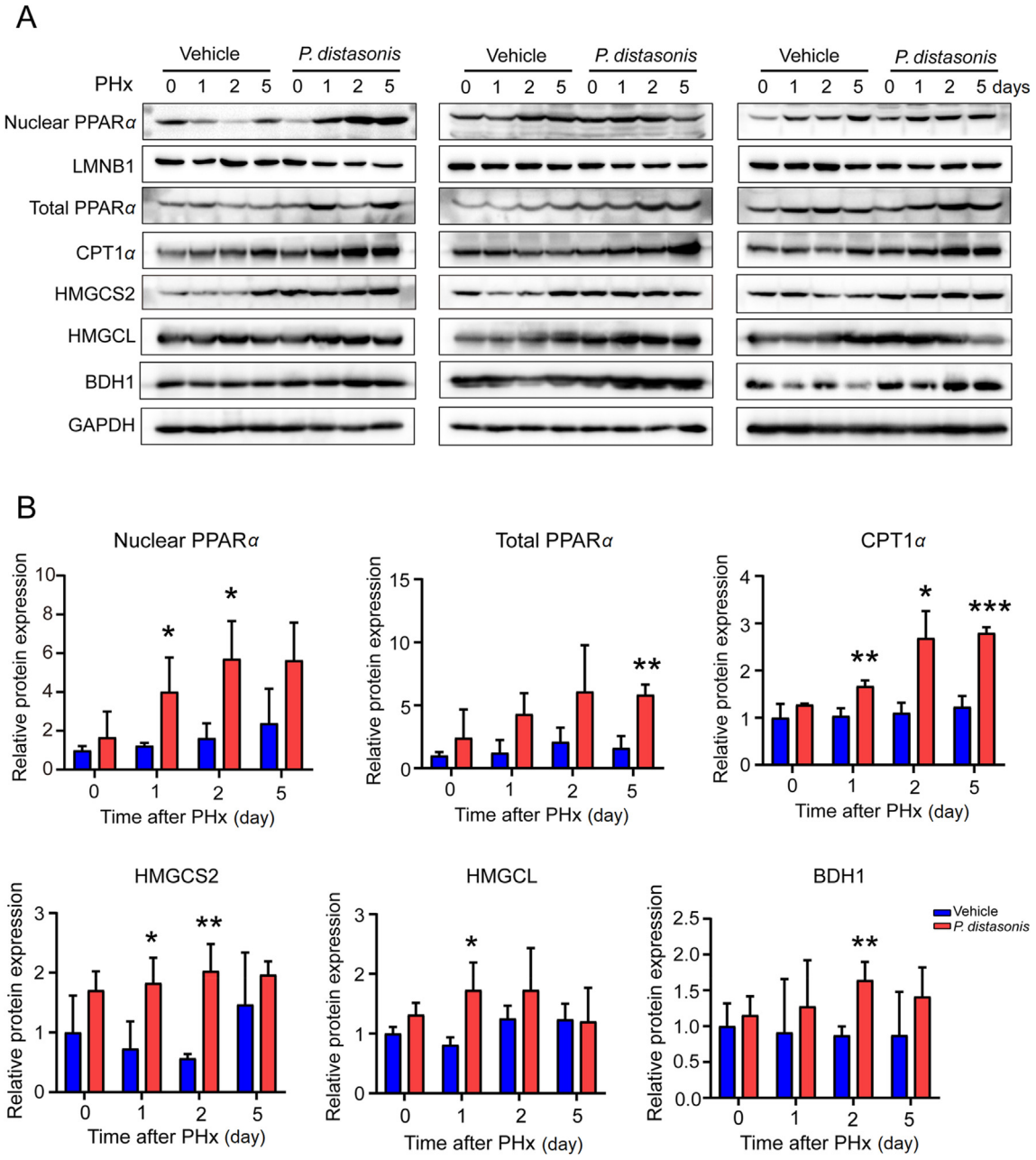

Figure 6 *P. distasonis* up-regulates the expression of fatty acid oxidation related proteins in livers after PHx. (A) Western blot analysis of nuclear PPARα, total PPARα, CPT1α, HMGCS2, HMGCSL and BDH1 in PHx mice after vehicle or LPD treatment ($n = 6$). (B) Quantification of the hepatic fatty acid oxidation related proteins expression. Data are presented as mean ± SD; *$P < 0.05$, **$P < 0.01$, ***$P < 0.001$ compared to the vehicle group.

F). Additionally, the expression of proliferation-related proteins, including CCNA1, CCND1 CCNE1 and CDK4 were increased in BHB-treated mice after PHx, but these effects were potently inhibited in BHB + Stattic-treated mice (Fig. 8G, Fig. S11B). These results indicated that BHB promoted liver regeneration potential through STAT3 signaling.

4. Discussion

PHx is the prominent clinical intervention for patients suffering from diverse end-stage liver diseases. Liver size and function have to be restored quickly post-PHx to achieve optimal patient outcomes and prognosis. Therefore, it is crucial to comprehend the mechanisms that control liver regeneration after PHx, which encompasses external factors transmitted through the gut−liver axis. Recent studies have shown that gut microbiota composition changes dynamically during liver regeneration and may affect liver tissue repair and regeneration after liver injury[17,18]. However, the key bacterial species involved in liver regeneration and the underlying mechanisms remain unclear. The current study clearly demonstrated that *P. distasonis* was the most significantly specific bacteria paralleling the dynamic change of hepatocyte proliferation and liver regeneration. Treatment with live *P. distasonis*

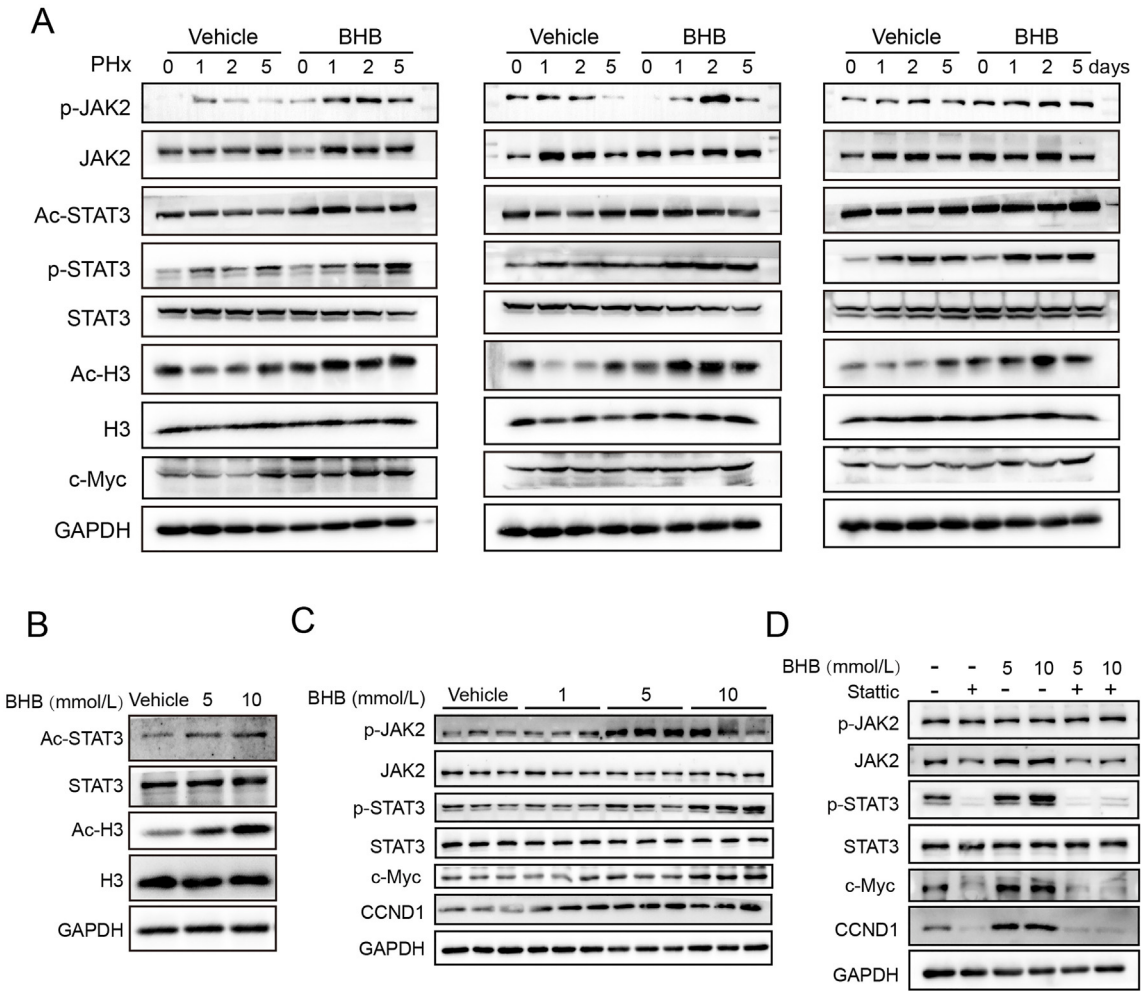

Figure 7 BHB promotes liver regeneration by activating the STAT3 signaling pathway *in vitro*. (A) Western blot analysis of p-JAK2, JAK2, Ac-STAT3, p-STAT3, STAT3, Ac-H3, H3 and c-Myc in PHx mice after vehicle or BHB treatment. (B) Western blot analysis of Ac-STAT3, STAT3, Ac-H3 and H3 in HepG2 cells treated with 5 or 10 mmol/L BHB for 3 h. (C) Western blot analysis of p-JAK2, JAK2, p-STAT3, STAT3 and proliferation protein in HepG2 cells treated with 1, 5 or 10 mmol/L BHB for 3 h. (D) Western blot analysis of p-JAK2, JAK2, p-STAT3, STAT3 and proliferation protein in HepG2 cells treated with static with or without BHB for 3 h.

significantly promoted hepatocyte proliferation and liver regeneration after PHx. Moreover, the metabolite BHB, which was positively associated with *P. distasonis*, also promoted liver regeneration after PHx. Mechanistically, *P. distasonis* boosted fatty acid oxidation, increased BHB production in the liver. BHB then activated STAT3 signaling and promoted liver regeneration after PHx. These findings provide a relevant argument for using *P. distasonis* or BHB as a potential strategy for promoting hepatic regeneration after PHx or transplantation.

P. distasonis is the Gram-negative obligate anaerobic strain belonging to the genus *Parabacteroides*, which commonly colonizes the gastrointestinal tract of numerous species[37]. Several previous studies have indicated that *P. distasonis* abundance is negatively correlated with liver disease severity[16,38]. The abundance of gut microbial is influenced by multiple factors, including bile acids produced in the liver, which can affect gut microbial growth. Specifically, hyodeoxycholic acid has been reported to create a favorable environment for the proliferation of *P. distasonis*, thereby improving non-alcoholic fatty liver disease[23]. The current study shows significant dynamic changes in *P. distasonis* abundance during liver regeneration, which may be regulated by bile acids or signals involved in bile acid homeostasis. Previous studies have found that *P. distasonis* prevents post-calorie restriction weight regain, improves obesity, ameliorates acute pancreatitis, colorectal cancer, liver fibrosis, and alcoholic hepatitis through regulating related metabolites such as ursodeoxycholic acid, lithocholic acid, succinate, acetate, and bile salt hydrolase[16,39,40]. Here, we have found that live *P. distasonis* can significantly promote hepatocyte proliferation and liver regeneration post-PHx by increasing the level of BHB in mouse liver, indicating that *P. distasonis* plays an important role in liver regeneration. It has been found that the cellular components of *P. distasonis* contribute differently to various diseases. The membrane fraction of *P. distasonis* prevents colon tumours, but does not alleviate obesity and refractory epilepsy in mice[41-43]. In this study, we found that KPD did not promote liver regeneration after PHx, suggesting that the cellular components of *Parabacteroides disasonis* may not contribute significantly to liver regeneration after PHx. Since studies on the role of *P. distasonis* in liver regeneration is limited, the present study provides novel insights for liver *P. distasonis* in promoting liver regeneration.

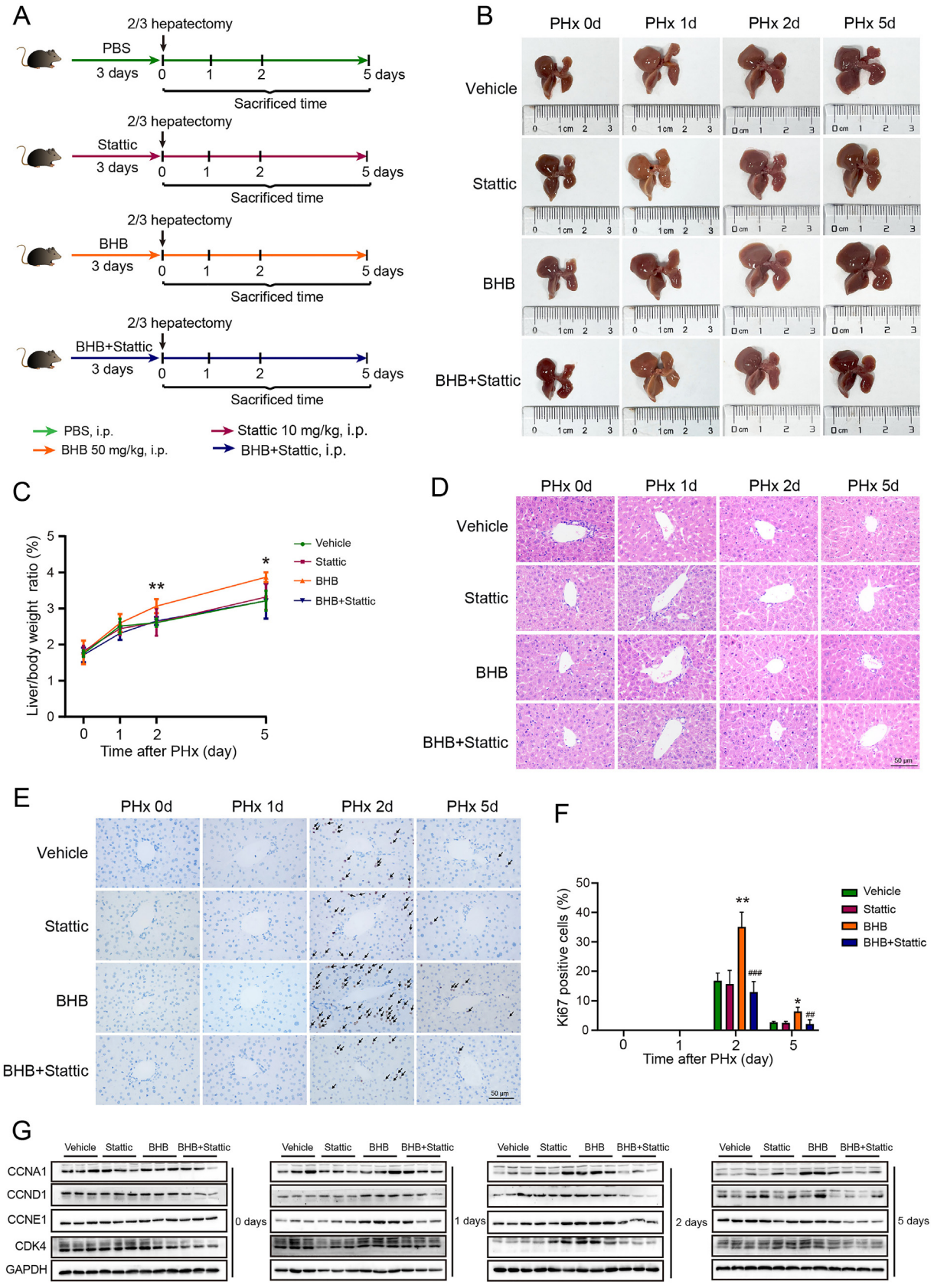

Figure 8 BHB promotes liver regeneration by activating the STAT3 signaling pathway *in vivo*. (A) Mice were intraperitoneally injected with Stattic (10 mg/kg/day) or BHB (50 mg/kg/day) or BHB + Stattic for 3 days and then subjected to PHx. Mice continued to be treated with Stattic (10 mg/kg/day) or BHB (50 mg/kg/day) or BHB + Stattic following PHx until the end of the study. (B) Representative liver images from PHx

Since *P. distasonis* primarily influences the liver microenvironment and improves liver diseases through the production or induction of host-derived metabolites, we performed targeted metabolomic analysis and found that the relative abundance of *P. distasonis* is significantly positively correlated with BHB concentration in cecal contents and liver post-PHx. Furthermore, *P. distasonis* significantly increased BHB levels in the liver post-PHx. However, we did not observe an increase in BHB levels in the *P. distasonis* culture medium *in vitro*, which is consistent with previous research findings[44]. These results suggest that *P. distasonis* may stimulate host metabolism to produce BHB. It has been reported that BHB is predominantly synthesized in the liver *via* fatty acid oxidation, and the gut microbiota plays a crucial role in modulating host lipid metabolism, which might contribute to BHB synthesis[45,46]. Leclercq et al.[47] found that the relative abundance of *P. distasonis* in the gut was significantly reduced in alcohol-dependent patients. At the same time, the inhibition of fatty acid oxidation in the liver was suppressed and the production of BHB was reduced, suggesting a potential association between *P. distasonis* and hepatic lipid metabolism[47]. However, the exact regulatory effect of *P. distasonis* on hepatic lipid metabolism remains unclear. The critical role of PPARα in hepatic lipid metabolism has been widely reported. Its downstream genes, CTP1α and HMGCS2, are key rate-limiting enzymes for fatty acid oxidation and hepatic BHB production, respectively. Therefore, the expression of genes related to fatty acid oxidation and BHB production was examined[48-50]. We showed that *P. distasonis* regulates the fatty acid oxidation pathway in the liver after PHx and significantly upregulates the protein levels of PPARα, CPT1α, HMGCS2, HMGCL, and BDH1. These results highlight a novel role for *P. distasonis* in regulating hepatic lipid metabolism and increasing hepatic BHB levels during liver regeneration after PHx.

BHB can not only be utilized as an energy substrate by extrahepatic tissues such as the heart, kidneys, and muscles, but also act as a signaling molecule and epigenetic factor to regulate physiological and pathological processes in the body[45]. In recent years, supplementation with exogenous BHB has been shown to have protective effects in liver diseases, such as liver ischemia−reperfusion injury, alcoholic liver disease, and immune-mediated hepatitis[51-53]. Moreover, BHB has been identified as a potential therapeutic target for non-alcoholic fatty liver disease[54]. In the present study, administration of BHB significantly promoted liver regeneration post-PHx. Moreover, compared to the vehicle group, BHB significantly reduced the levels of ALP on Day 1 and ALT on Day 2 in serum post-PHx, suggesting that BHB promotes the recovery of liver function post-PHx[51]. These findings are consistent with previous reports demonstrating that BHB reduces hepatocellular necrosis in mouse models of liver ischemia−reperfusion injury and alcoholic liver disease, and further confirms the role of BHB in ameliorating liver injury in a novel model of liver regeneration. On the other hand, the current study showed that HDCA and 3HPA treatment did not increase the liver size and liver/body weight ratio on Day 2 post-PHx, suggesting that HDCA and 3HPA could not promote liver regeneration after PHx.

The critical role of the IL-6−JAK2−STAT3 axis in hepatocyte proliferation and liver regeneration after PHx has been well-established. In the present study, administration of BHB upregulated liver regeneration initiating cytokine IL-6 and downstream p-JAK2, p-STAT3, CCND1 and c-Myc levels. The nuclear translocation and transactivation activity of STAT3 is also regulated by acetylation at lysine residue 685[36]. We found that BHB also upregulated ac-STAT3 levels. Additionally, BHB could promote hepatocyte proliferative and liver regeneration by the STAT3 signaling pathway *in vitro* and *in vivo*. On the other hand, reports have shown that BHB exerts anti-inflammatory effects by inhibiting IL-6 and the STAT3 signaling pathway in mouse models of Parkinson's disease and radiation proctopathy[55,56]. However, some studies have suggested that BHB upregulates IL-6 expression by modulating the activation of the NF-κB signaling pathway in primary alveolar macrophages and calf hepatocytes[57,58]. These inconsistencies suggest that the regulation of STAT3 signaling by BHB may vary across different disease models. Nevertheless, the specific mechanisms involved still require further investigation.

5. Conclusions

In conclusion, this study identified for the first time that *P. distasonis* and its metabolite BHB significantly promote liver regeneration after PHx. Furthermore, this study revealed a novel mechanism that *P. distasonis* promotes liver regeneration via enhancing hepatic fatty acid oxidation, increasing BHB production in the liver, and then triggering BHB-driven STAT3 signaling activation. These findings provide novel insights for the use of *P. distasonis* or BHB as a potential strategy to promote liver regeneration after PHx.

Acknowledgments

The work was supported by the National Key R&D Program of China (2022YFA1104900), the National Natural Science Foundation of China (Grant numbers: 82025034, U23A20535, 82404738 and 82404730), the Shenzhen Science and Technology Program (KQTD20190929174023858, China), the Science and Technology Innovation Project of Guangdong Medical Products Administration (Grant number: 2023ZDZ06, China), and the Local Innovative and Research Teams Project of Guangdong Pearl River Talents Program (Grant number: 2017BT01Y093, China).

Author contributions

Manlan Guo: Writing − original draft, Visualization, Validation, Data curation. Xiaowen Jiang: Writing − original draft, Validation. Hui Ouyang: Validation. Xianglong Zhang: Software. Shuaishuai Zhang: Validation. Peng Wang: Software, Methodology. Guofang Bi: Validation. Ting Wu: Validation. Wenhong Zhou: Validation. Fengting Liang: Validation. Xiao Yang: Supervision. Shicheng Fan: Writing − review & editing. Jian-hong Fang: Writing − review & editing. Peng Chen: Supervision, Writing − review & editing. Huichang Bi: Writing − review & editing, Supervision, Project administration, Conceptualization.

mice after vehicle or Stattic or BHB or BHB + Stattic administration. (C) Liver/body weight ratios ($n = 6$), (D) H&E and (E) Ki67 staining liver tissues from PHx mice ($n = 3$). (F) Quantification of the number of Ki67$^+$ cells ($n = 6$). (G) Western blotting analysis of the proliferation-related proteins CCNA1, CCND1, CCNE1 and CDK4 in PHx mice after vehicle or Stattic or BHB or BHB + Stattic administration ($n = 6$). Data are presented as mean ± SD; *$P < 0.05$, **$P < 0.01$ compared to the vehicle group at the same time point; ##$P < 0.01$, ###$P < 0.001$ compared to the BHB group at the same time point. Scale bar = 50 μm.

Conflicts of interest

The authors declare no competing interests.

Appendix A. Supporting information

Supporting information to this article can be found online at https://doi.org/10.1016/j.apsb.2025.01.024.

References

1. Forbes SJ, Newsome PN. Liver regeneration—mechanisms and models to clinical application. *Nat Rev Gastroenterol Hepatol* 2016;**13**:473–85.
2. Michalopoulos GK. Hepatostat: liver regeneration and normal liver tissue maintenance. *Hepatology* 2017;**65**:1384–92.
3. Michalopoulos GK. Liver regeneration. *J Cell. Physiol* 2007;**213**:286–300.
4. Huh CG, Factor VM, Sánchez A, Uchida K, Conner EA, Thorgeirsson SS. Hepatocyte growth factor/c-met signaling pathway is required for efficient liver regeneration and repair. *Proc Nat Acad Sci U S A* 2004;**101**:4477–82.
5. Ozaki M, Haga S, Zhang HQ, Irani K, Suzuki S. Inhibition of hypoxia/reoxygenation-induced oxidative stress in HGF-stimulated antiapoptotic signaling: role of PI3-K and Akt kinase upon rac1. *Cell Death Differ* 2003;**10**:508–15.
6. Fan S, Gao Y, Qu A, Jiang Y, Li H, Xie G, et al. YAP–TEAD mediates PPAR α-induced hepatomegaly and liver regeneration in mice. *Hepatology* 2022;**75**:74–88.
7. Wu X, Sun R, Chen Y, Zheng X, Bai L, Lian Z, et al. Oral ampicillin inhibits liver regeneration by breaking hepatic innate immune tolerance normally maintained by gut commensal bacteria. *Hepatology* 2015;**62**:253–64.
8. Yin Y, Sichler A, Ecker J, Laschinger M, Liebisch G, Höring M, et al. Gut microbiota promote liver regeneration through hepatic membrane phospholipid biosynthesis. *J Hepatol* 2023;**78**:820–35.
9. Knight DJ, Girling KJ. Gut flora in health and disease. *Lancet* 2003;**361**:1831.
10. Gasaly N, de Vos P, Hermoso MA. Impact of bacterial metabolites on gut barrier function and host immunity: a focus on bacterial metabolism and its relevance for intestinal inflammation. *Front Immunol* 2021;**12**:658354.
11. Rifatbegovic Z, Mesic D, Ljuca F, Zildzic M, Avdagic M, Grbic K, et al. Effect of probiotics on liver function after surgery resection for malignancy in the liver cirrhotic. *Med Arh* 2010;**64**:208–11.
12. Rayes N, Pilarski T, Stockmann M, Bengmark S, Neuhaus P, Seehofer D. Effect of pre- and probiotics on liver regeneration after resection: a randomised, double-blind pilot study. *Benef Microbe* 2012;**3**:237–44.
13. Liu Y, Chen K, Li F, Gu Z, Liu Q, He L, et al. Probiotic *Lactobacillus rhamnosus* GG prevents liver fibrosis through inhibiting hepatic bile acid synthesis and enhancing bile acid excretion in mice. *Hepatology* 2020;**71**:2050–66.
14. Grander C, Adolph TE, Wieser V, Lowe P, Wrzosek L, Gyongyosi B, et al. Recovery of ethanol-induced *Akkermansia muciniphila* depletion ameliorates alcoholic liver disease. *Gut* 2018;**67**:891–901.
15. Wang H, Wang Q, Yang C, Guo M, Cui X, Jing Z, et al. *Bacteroides acidifaciens* in the gut plays a protective role against CD95-mediated liver injury. *Gut Microbes* 2022;**14**:2027853.
16. Zhao Q, Dai MY, Huang RY, Duan JY, Zhang T, Bao WM, et al. *Parabacteroides distasonis* ameliorates hepatic fibrosis potentially *via* modulating intestinal bile acid metabolism and hepatocyte pyroptosis in male mice. *Nat Commun* 2023;**14**:1829.
17. Bao Q, Yu L, Chen D, Li L. Variation in the gut microbial community is associated with the progression of liver regeneration. *Hepatol Res* 2020;**50**:121–36.
18. Liu HX, Rocha CS, Dandekar S, Wan YJ. Functional analysis of the relationship between intestinal microbiota and the expression of hepatic genes and pathways during the course of liver regeneration. *J Hepatol* 2016;**64**:641–50.
19. Li X, Sun J, Fan X, Guan L, Li D, Zhou Y, et al. Schisandrol B promotes liver regeneration after partial hepatectomy in mice. *Eur J Pharmacol* 2018;**818**:96–102.
20. Mitchell C, Willenbring H. A reproducible and well-tolerated method for 2/3 partial hepatectomy in mice. *Nat Protoc* 2008;**3**:1167–70.
21. Trotta MC, Gesualdo C, Herman H, Gharbia S, Balta C, Lepre CC, et al. Systemic beta-hydroxybutyrate affects BDNF and autophagy into the retina of diabetic mice. *Int J Mol Sci* 2022;**23**:10184.
22. Pan A, Sun XM, Huang FQ, Liu JF, Cai YY, Wu X, et al. The mitochondrial β-oxidation enzyme HADHA restrains hepatic glucagon response by promoting β-hydroxybutyrate production. *Nat Commun* 2022;**13**:386.
23. Kuang J, Wang J, Li Y, Li M, Zhao M, Ge K, et al. Hyodeoxycholic acid alleviates non-alcoholic fatty liver disease through modulating the gut–liver axis. *Cell Metab* 2023;**35**:1752–66.e8.
24. Jin S, Chen P, Yang J, Li D, Liu X, Zhang Y, et al. *Phocaeicola vulgatus* alleviates diet-induced metabolic dysfunction-associated steatotic liver disease progression by downregulating histone acetylation level *via* 3-HPAA. *Gut Microbes* 2024;**16**:2309683.
25. Latourte A, Cherifi C, Maillet J, Ea HK, Bouaziz W, Funck-Brentano T, et al. Systemic inhibition of IL-6/Stat3 signalling protects against experimental osteoarthritis. *Ann Rheum Dis* 2017;**76**:748–55.
26. Youm YH, Nguyen KY, Grant RW, Goldberg EL, Bodogai M, Kim D, et al. The ketone metabolite β-hydroxybutyrate blocks NLRP3 inflammasome-mediated inflammatory disease. *Nat Med* 2015;**21**:263–9.
27. Fu H, Dong R, Zhang Y, Xu J, Liu M, Chen P. Tmub1 negatively regulates liver regeneration *via* inhibiting STAT3 phosphorylation. *Cell Signal* 2019;**55**:65–72.
28. Jiang Y, Feng D, Ma X, Fan S, Gao Y, Fu K, et al. Pregnane X receptor regulates liver size and liver cell fate by Yes-associated protein activation in mice. *Hepatology* 2019;**69**:343–58.
29. Li X, Fan S, Cai C, Gao Y, Wang X, Zhang Y, et al. YAP regulates the liver size during the fasting-refeeding transition in mice. *Acta Pharm Sin B* 2023;**13**:1588–99.
30. Gong S, Lan T, Zeng L, Luo H, Yang X, Li N, et al. Gut microbiota mediates diurnal variation of acetaminophen induced acute liver injury in mice. *J Hepatol* 2018;**69**:51–9.
31. Hu J, Luo H, Wang J, Tang W, Lu J, Wu S, et al. Enteric dysbiosis-linked gut barrier disruption triggers early renal injury induced by chronic high salt feeding in mice. *Exp Mol Med* 2017;**49**:e370.
32. Bolyen E, Rideout JR, Dillon MR, Bokulich NA, Abnet CC, Al-Ghalith GA, et al. Reproducible, interactive, scalable and extensible microbiome data science using QIIME 2. *Nat Biotechnol* 2019;**37**:852–7.
33. Zhang S, Guo M, Jiang X, Tang L, Wu T, Bi G, et al. PXR triggers YAP–TEAD binding and Sirt2-driven YAP deacetylation and polyubiquitination to promote liver enlargement and regeneration in mice. *Pharmacol Res* 2023;**188**:106666.
34. Cheng CW, Biton M, Haber AL, Gunduz N, Eng G, Gaynor LT, et al. Ketone body signaling mediates intestinal stem cell homeostasis and adaptation to diet. *Cell* 2019;**178**:1115–31.e15.
35. Cressman DE, Diamond RH, Taub R. Rapid activation of the Stat3 transcription complex in liver regeneration. *Hepatology* 1995;**21**:1443–9.
36. Yuan ZL, Guan YJ, Chatterjee D, Chin YE. Stat3 dimerization regulated by reversible acetylation of a single lysine residue. *Science* 2005;**307**:269–73.
37. Sakamoto M, Benno Y. Reclassification of *Bacteroides distasonis*, *Bacteroides goldsteinii* and *Bacteroides merdae* as *Parabacteroides distasonis* gen. nov., comb. nov., *Parabacteroides goldsteinii* comb. nov. and *Parabacteroides merdae* comb. nov. *Int J Syst Evol Microbiol* 2006;**56**:1599–605.

38. Wei W, Wong CC, Jia Z, Liu W, Liu C, Ji F, et al. *Parabacteroides distasonis* uses dietary inulin to suppress NASH *via* its metabolite pentadecanoic acid. *Nat Microbiol* 2023;**8**:1534−48.
39. Li M, Wang S, Li Y, Zhao M, Kuang J, Liang D, et al. Gut microbiota-bile acid crosstalk contributes to the rebound weight gain after calorie restriction in mice. *Nat Commun* 2022;**13**:2060.
40. Ezeji JC, Sarikonda DK, Hopperton A, Erkkila HL, Cohen DE, Martinez SP, et al. *Parabacteroides distasonis*: intriguing aerotolerant gut anaerobe with emerging antimicrobial resistance and pathogenic and probiotic roles in human health. *Gut Microbes* 2021;**13**:1922241.
41. Wang K, Liao M, Zhou N, Bao L, Ma K, Zheng Z, et al. *Parabacteroides distasonis* alleviates obesity and metabolic dysfunctions *via* production of succinate and secondary bile acids. *Cell Rep* 2019;**26**:222−35.e5.
42. Olson CA, Vuong HE, Yano JM, Liang QY, Nusbaum DJ, Hsiao EY. The gut microbiota mediates the anti-seizure effects of the ketogenic diet. *Cell* 2018;**173**:1728−41.e13.
43. Kverka M, Zakostelska Z, Klimesova K, Sokol D, Hudcovic T, Hrncir T, et al. Oral administration of *Parabacteroides distasonis* antigens attenuates experimental murine colitis through modulation of immunity and microbiota composition. *Clin Exp Immunol* 2011;**163**:250−9.
44. Mao T, Qin F, Zhang M, Li J, Li J, Lai M. Elevated serum β-hydroxybutyrate, a circulating ketone metabolite, accelerates colorectal cancer proliferation and metastasis *via* ACAT1. *Oncogene* 2023;**42**:1889−99.
45. Newman JC, Verdin E. Ketone bodies as signaling metabolites. *Trend Endocrinol Metab* 2014;**25**:42−52.
46. Shen H, Zhou L, Zhang H, Yang Y, Jiang L, Wu D, et al. Dietary fiber alleviates alcoholic liver injury *via Bacteroides acidifaciens* and subsequent ammonia detoxification. *Cell Host Microbe* 2024;**32**:1331−46.e6.
47. Leclercq S, Le Roy T, Furgiuele S, Coste V, Bindels LB, Leyrolle Q, et al. Gut microbiota-induced changes in β-hydroxybutyrate metabolism are linked to altered sociability and depression in alcohol use disorder. *Cell Rep* 2020;**33**:108238.
48. Grabacka M, Pierzchalska M, Dean M, Reiss K. Regulation of ketone body metabolism and the role of PPAR. *A Int J Mol Sci* 2016;**17**:2093.
49. Hao F, Tian M, Zhang X, Jin X, Jiang Y, Sun X, et al. Butyrate enhances CPT1A activity to promote fatty acid oxidation and iTreg differentiation. *Proc Nat Acad Sci U S A* 2021;**118**:e2014681118.
50. Wang Q, Zhou Y, Rychahou P, Fan TW, Lane AN, Weiss HL, et al. Ketogenesis contributes to intestinal cell differentiation. *Cell Death Differ* 2017;**24**:458−68.
51. Miyauchi T, Uchida Y, Kadono K, Hirao H, Kawasoe J, Watanabe T, et al. Up-regulation of FOXO1 and reduced inflammation by β-hydroxybutyric acid are essential diet restriction benefits against liver injury. *Proc Nat Acad Sci U S A* 2019;**116**:13533−42.
52. Chen Y, Ouyang X, Hoque R, Garcia-Martinez I, Yousaf MN, Tonack S, et al. β-Hydroxybutyrate protects from alcohol-induced liver injury *via* a Hcar2−cAMP dependent pathway. *J Hepatol* 2018;**69**:687−96.
53. Hazem SH, Hamed MF, Saad MA, Gameil NM. Comparison of lactate and β-hydroxybutyrate in the treatment of concanavalin-A induced hepatitis. *Int Immunopharmacol* 2018;**61**:376−84.
54. Tendler D, Lin S, Yancy Jr WS, Mavropoulos J, Sylvestre P, Rockey DC, et al. The effect of a low-carbohydrate, ketogenic diet on nonalcoholic fatty liver disease: a pilot study. *Dig Dis Sci* 2007;**52**:589−93.
55. Ge Z, Chen C, Chen J, Jiang Z, Chen L, Wei Y, et al. Gut microbiota-derived 3-hydroxybutyrate blocks GPR43-mediated IL6 signaling to ameliorate radiation proctopathy. *Adv Sci* 2024;**11**:e2306217.
56. Jiang Z, Yin X, Wang M, Wang Y, Li F, Gao Y, et al. β-Hydroxybutyrate alleviates pyroptosis in MPP^+/MPTP-induced Parkinson's disease models *via* inhibiting STAT3/NLRP3/GSDMD pathway. *Int Immunopharmacol* 2022;**113**:109451.
57. Qi J, Yang Q, Xia Q, Huang F, Guo H, Cui H, et al. Low glucose plus β-hydroxybutyrate induces an enhanced inflammatory response in Yak alveolar macrophages *via* activating the GPR109A/NF-κB signaling pathway. *Int J Mol Sci* 2023;**24**:11331.
58. Hwang CY, Choe W, Yoon KS, Ha J, Kim SS, Yeo EJ, et al. Molecular mechanisms for ketone body metabolism, signaling functions, and therapeutic potential in cancer. *Nutrients* 2022;**14**:4932.